Magneto-Reactive Jeffrey Nanofluid Flow over a Stretching Sheet with Activation Energy, Nonlinear Thermal Radiation and Entropy Analysis

Ephesus Fatunmbi[1], Jamiu Badru[2]& Abayomi Oke[3]
[1-2]Department of Mathematics and Statistics
Federal Polytechnic, Ilaro, Nigeria.
[3]Department of Mathematics and Actuarial Sciences
Kenyatta University, Kenya
ephesus.fatunmbi@federalpolyilaro.edu.ng, jamiu.badru@federalpolyilaro.edu.ng
okeabayomisamuel@gmail.com

ABSTRACT
This article investigates the flow of an electrically conducting and chemically reactive Jeffery nanofluid confined in a two-dimensional permeable stretching sheet in a porous medium. The mathematical model developed for the flow is influenced by nonlinear thermal radiation, viscous dissipation coupled with non-uniform heat source, activation energy and entropy analysis. Similarity transformation variables are used to translate the nonlinear partial differential equations to ordinary differential equations and then solved via Runge-Kutta-Fehlberg algorithm associated with shooting technique. The significant contributions of the emerging physical parameters are graphically and tabularly discussed while the computational values of selected parameters agree perfectly with earlier published studies in the limiting conditions. The current study shows that the velocity profiles advances with an uplift in the Deborah number and stretching parameter while the heat transfer improves with a hike in the surface convection term. More so, the entropy generation rises with frictional heating and magnetic parameters while it depletes with a boost in the thermophoresis term. More so, heat transfer improves with velocity ratio term, radiation and Prandtl numbers as the thermophoresis influence raises the nanoparticles concentration field.

Keywords: Activation energy; Entropy analysis; Nonlinear thermal radiation; Jeffery nanofluid; Stretching sheet

1. INTRODUCTION

The studies of non-Newtonian fluids have become a sought-after and popular research field for the scientists, engineers and researchers in the recent times due to unparalleled and unquantifiable applications derivable from such investigations. Common applications are often found in engineering and manufacturing processes, such as in food processing, polymer, plastics and textiles manufacturing, oil drilling, etc. (Madhu and Kishan, 2015). Due to complexity in the properties of non-Newtonian fluids, it is quite difficult to describe the characteristics features of the non-Newtonian fluids in a single constitutive model. In view of this, there are several non-Newtonian fluid models formulated to capture various fluid attributes, such models include the Jeffrey fluids, Maxwell fluid, Williamson fluids, Eyring-Powell fluids, etc. (Dalir *et al.*, 2015; Ramesh, 2018, Shah *et al.*, 2020). Jeffery fluids exhibits the features of the viscoelastic type with the properties of relaxation and retardation times.

Conventional base fluids such as water, oil, ethanol glycol, etc. have been found to be of low thermal conductivity and thus offer low heat transfer rates. A new class of heat transfer fluid originated by Choi and Eastman (1995) is known as nanofluid. Nanofluid describes the suspension of nanometer particles in base fluids for an improved thermal conductivity in comparison to the traditional fluids. With such composition, there is an improved thermal conductivity as well as heat transfer required in various engineering and manufacturing devices such as in pharmaceutical industries, transportation industries, cooling of engines and vehicles, refrigerator, chiller (see Prasannakumara et al., 2017; Ibrahim and Gamachu, 2019; Fatunmbi and Adeshina, 2020). The investigations of boundary layer flows induced by stretching sheet offer significant engineering and industrial usage such as encountered in extrusion metal and plastics, wire drawing, crystal growing, textile and paper production, etc. (Akinbobola and Okoya, 2015; Fatunmbi and Adeniyan, 2018; Fatunmbi and

Okoya, 2020). The pioneering work was conducted by Crane (1970) while extended versions of such a study on different configurations and boundary conditions have been widely analyzed by various researchers. Nadeem *et al.* (2011), Shateyi and Gerald (2018), Fatunmbi and Okoya (2020).

Many of the aforementioned investigators have restricted themselves to the analysis of thermodynamics first law whereas entropy generations derivable from the thermodynamic second law is crucial in measuring the level of disorderliness or chaos in a thermodynamical system. The extent of energy decay that occurs in a thermodynamical system can be measured by entropy analysis, thus to optimize the available energy in thermal engineering devices, the factors aiding the destruction of energy must be identified and minimized. Besides, the processes of heating and cooling occur frequently in many engineering and manufacturing processes and in such cases, the development of thermal engineering appliances becomes crucial. For such gadgets to perform optimally, the minimization of entropy production becomes essential (Bejan, 1982,1986; Salawu and Fatunmbi, 2017; Pal *et al.* 2019)).

In view of the literature analysis above, the current study therefore is embarked upon to investigate the flow of a reactive Jeffery nanofluid over a stretching sheet in a confined porous medium with entropy generation analysis, nonlinear thermal radiation, activation energy and in the neighborhoud of a stagnation point. These are crucial parameters of engineering and industrial usefulness which have been ignored by the previous authors that have been incorporated in the current study.

1. PROBLEM FORMULATION AND MODELLING

As depicted in Fig. 1, the flow is assumed to be two-dimensional, incompressible and steady with (x, y) as the coordinate system. The flow is towards x axis while y axis is perpendicular to it. The hydromagnetic Jeffery nanofluid flows along a permeable stretchable sheet in the neighbourhood of a stagnation point.

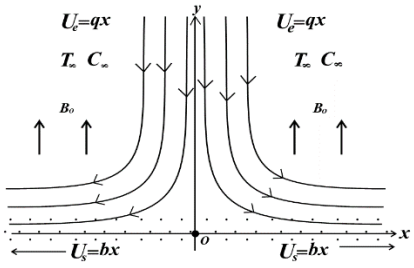

Fig. 1 Flow Geometry

Two equal but opposite forces are imposed parallel to the stretching axis so that the sheet is stretched with the origin being fixed at $y = 0$ and the fluid pervades the region $y \geq 0$ At the stretching sheet, the velocity is U_s whereas at the upstream it takes the form $u \to U_e$. An externally applied uniform magnetic field $B(x) = B_0$ is directed normal to axis of flow and without considering the impact of the induced magnetic due to sufficiently low Reynolds number. The sheet temperature is aided through a convective heating mechanism from a hot fluid with a temperature T_f. The thermal field features Joule heating, non-uniform heat source/sink, viscous and Darcy dissipation together with nonlinear thermal radiation coupled with thermophoresis and Brownian diffusion effects whereas the nanoparticle concentration field is developed with the influence of chemical reaction and activation energy.

With the stated assumptions and using the usual boundary approximations, the governing transport equations for the problem under consideration are listed below.

$$\frac{\partial u}{\partial x} + \frac{\partial v}{\partial y} = 0, \tag{1}$$

$$u\frac{\partial u}{\partial x}+v\frac{\partial u}{\partial y}=-\frac{1}{\rho}\frac{\partial p}{\partial x}+\frac{\mu}{\rho(1+\beta)}\left[\frac{\partial^2 u}{\partial y^2}+\alpha\left(u\frac{\partial^3 u}{\partial x\partial y^2}-\frac{\partial u}{\partial x}\frac{\partial^2 u}{\partial y^2}+\frac{\partial u}{\partial y}\frac{\partial^2 u}{\partial x\partial y}+v\frac{\partial^3 u}{\partial y^3}\right)\right]-\frac{v}{K^*}u-\frac{\sigma B_0^2}{\rho}u, \tag{2}$$

where

$$U_e\frac{dU_e}{dx}=-\frac{1}{\rho}\frac{\partial p}{\partial x}-\frac{v}{K^*}U_e-\frac{\sigma B_0^2}{\rho}U_e \tag{3}$$

Hence, Eq. (2) yields

$$u\frac{\partial u}{\partial x}+v\frac{\partial u}{\partial y}=U_e\frac{dU_e}{dx}+\frac{\mu\left[\frac{\partial^2 u}{\partial y^2}+\alpha\left(u\frac{\partial^3 u}{\partial x\partial y^2}-\frac{\partial u}{\partial x}\frac{\partial^2 u}{\partial y^2}+\frac{\partial u}{\partial y}\frac{\partial^2 u}{\partial x\partial y}+v\frac{\partial^3 u}{\partial y^3}\right)\right]}{\rho(1+\beta)}-\frac{U_e v(u-U_e)}{K^*}\frac{dU_e}{dx}-\frac{\sigma B_0^2(u-U_e)}{\rho}, \tag{4}$$

$$u\frac{\partial T}{\partial x}+v\frac{\partial T}{\partial y}=\frac{k}{\rho c_p}\frac{\partial^2 T}{\partial y^2}+\tau\left[\frac{D_T}{T_\infty}\left(\frac{\partial T}{\partial y}\right)^2+D_B\left(\frac{\partial T}{\partial y}\frac{\partial C}{\partial y}\right)\right]+\frac{v}{c_p K^*}(u-U_e)^2+\frac{\sigma B_0^2}{\rho c_p}(u-U_e)^2+\frac{v}{c_p}\left(\frac{\partial u}{\partial y}\right)^2+\frac{16\sigma^*}{3k_*\rho c_p}\left(T^3\frac{\partial^2 T}{\partial y^2}+3T^2\left(\frac{\partial T}{\partial y}\right)^2\right)+\frac{q'''}{\rho c_p}, \tag{5}$$

$$u\frac{\partial C}{\partial x}+v\frac{\partial C}{\partial y}=D_B\frac{\partial C^2}{\partial y^2}+\frac{D_T}{T_\infty}\left(\frac{\partial^2 T}{\partial y^2}\right)-K_r^2(C-C_\infty)\left(\frac{T}{T_\infty}\right)^n\exp\left(-\frac{E_0}{\delta T}\right). \tag{6}$$

The governing equations are accompanied with the following boundary conditions:

$$u=U_s=bx, v=V_w, -k\frac{\partial T}{\partial y}=h_T\left(T_f-T_\infty\right), -D_B\frac{\partial C}{\partial y}=h_m\left(C_f-C_\infty\right)\ at\ y=0,$$
$$u\to U_e=qx, \frac{\partial u}{\partial y}\longrightarrow 0, T\longrightarrow T_\infty, C\longrightarrow C_\infty,\ \ as\ \ y\to\infty. \tag{7}$$

The term q''' in Eq. (5) describes the non-uniform heat source/sink expressed as

$$q'''=\frac{kU_s}{xv}\left[Q(T_f-T_\infty)h'+Q^*(T-T_\infty)\right]. \tag{8}$$

In Eqs (1-8), u, v. Are the velocity components in x, y directions respectively. Also, $v, \mu, \rho, \alpha, k, D_B, D_T, T, C, Q/Q^\star$. respectively denotes kinematic viscosity, dynamic viscosity, density, relaxation time, thermal conductivity, Brownian diffusion coefficient, Thermophoretic diffusion, temperature, concentration, space dependent/temperature heat source. Similarly, $T_f, k^\star, E_0, b, h_t, C_f, \sigma^\star, \delta, \beta, K^*, h_m$ and τ orderly denote surface temperature, mean absorption coefficient, activation energy, stretching constant, coefficient of heat transfer, surface concentration, Stefan-Boltzmann constant, Boltzmann constant,, ratio of relaxation to retardation time, permeability of the porous medium, mass transfer coefficient, ratio of nanoparticle heat capacity to heat capacity of the fluid.

2.1 The Entropy Generation Equation

The volumetric rate of entropy generation for the nonlinear radiative, dissipative and electrically conducting Jeffery nanofluid is developed via the second law of thermodynamics as (see Fatunmbi and Adeniyan, 2020).

$$S_G=\frac{1}{T^2}\left(k+\frac{16\sigma^* T^3}{3k^* k}\right)\left(\frac{\partial T}{\partial y}\right)^2+\frac{\mu}{T}\left(\frac{\partial u}{\partial y}\right)^2+\frac{1}{T}\left(\sigma B_0^2+\frac{\mu}{K^*}\right)u^2+\frac{RD_B}{C}\left(\frac{\partial C}{\partial y}\right)^2+\frac{RD_B}{T}\left(\frac{\partial C}{\partial y}\frac{\partial T}{\partial y}\right). \tag{9}$$

The quantities in Eq. (10) are substituted into the governing equations to obtain the ordinary differential equations (11-13)

$$\eta = \sqrt{\frac{b}{v}}y, u = bxh'(\eta), v = \sqrt{bv}h(\eta), T = (T_f - T_\infty)\theta(\eta) + T_\infty,$$
$$C = (C_s - C_\infty)\theta(\xi) + C_\infty, u = \frac{\partial\psi}{\partial y}, v = -\frac{\partial\psi}{\partial x}. \tag{10}$$

$$h''' + (1+\beta)(hh'' - h'^2) + \zeta(h'^2 - hh'''') + (1+\beta)A^2 - (1+\beta)[M + Da](h' - A) = 0, \tag{11}$$

$$[1 + Rd(\theta_r - 1)\theta)^3\theta]\theta'' + 3Rd(\theta_r - 1)\theta'^2(1 + (\theta_r - 1)\theta)^2 + PrEc(M + Da)(h' - A)^2 +$$
$$+(Qh' + Q^*\theta) + Pr[h\theta' + Ech''^2 + Nt\theta'^2 + Nb\theta'\phi' + MEch'^2] += 0, \tag{12}$$

$$\phi'' + \frac{Nt}{Nb}\theta'' + Sch\phi' - Sc\gamma_1[1 + (\theta r - 1)\theta]^n \exp\left(-\frac{E}{1+(\theta r-1)\theta}\right)\phi = 0, \tag{13}$$

The transformed boundary conditions are:

$$h'(0) = 1, h(0) = Fw, 0'(0) = -G_1(1 - \theta(0)), \phi'(0) = -G_2(1 - \phi(0))$$
$$h'(\infty) = A, h''(\infty) = 0, \theta(\infty) = 0, \phi(\infty) = 0. \tag{14}$$

The dimensionless entropy generation also becomes

$$N_G = \frac{Re[1+Rd(1+(\theta r-1)\theta)^3]}{(1+(\theta_w-1)\theta)^2}\theta'^2 + \frac{PrEcRe(h''^2 + Mh'^2 + Da\,h'^2)}{(1+(\theta r-1)\theta)(\theta r-1)} +$$
$$\left(\frac{\gamma_2 Re(\phi_w-1)}{(\theta r-1)}\right)\left[\frac{(\phi_w-1)}{(1+(\phi_w-1)\phi)(\theta r-1)}\phi'^2 + \frac{1}{(1+(\theta r-1)\theta)}\phi'\theta'\right] = 0 \tag{15}$$

Where $N_G = \frac{S_G}{E'''}$ is the entropy number and E''' defines the characteristic entropy generation and S_G.is the entropy generation. In Eq. (15), the entropy generation is as a result of heat transfer (HT), fluid friction and magnetic/Ohmic heating (FFM) and diffusion/mass transfer effects (DIR). These sources are respectively indicated by the first, second and third terms of the RHS of Eq. (15). Furthermore, the significant input of each of these sources is measured by the Bejan number Be. This parameter describes the ratio of entropy generation as a result of heat and mass transfer to the entropy generation number

$$. Be = \frac{HT+DIR}{N_G} = \frac{HT+DIR}{HT+FFM+DIR}. \tag{16}$$

$$\theta r = \frac{T_f}{T_\infty}, Pr = \frac{\mu c_p}{k}, M = \frac{\sigma B_0^2}{b\rho}, Fw = \frac{V_w}{\sqrt{bv}}, Rd = \frac{16\sigma^* T_\infty^3}{3k^* k}, \zeta = b\alpha, Ec = \frac{U_s^2}{C_p(T_f - T_\infty)},$$
$$Sc = \frac{\nu}{D_B}, \gamma_1 = \frac{K_r^2}{b}, E = \frac{E_0}{\delta T_\infty}, G_1 = \frac{h_f}{k}\sqrt{\frac{\nu}{b}}, Nb = \tau\frac{D_B(C_w - C_\infty)}{\nu_\infty}, Nt = \tau\frac{D_T(T_f - T_\infty)}{T_\infty \nu}, \tag{17}$$
$$A = \frac{q}{b}, G_2 = \frac{h_2}{D_B}\sqrt{\frac{\nu}{b}}, \phi_w = \frac{C_s}{C_\infty}, Re = \frac{U_s x}{\nu_\infty}, D_a = \frac{\nu}{bK_0}, N_G = \frac{S_G}{E'''}.$$

Where the terms in Eq. (17) are orderly described as temperature ratio parameter, Prandtl number , magnetic field , suction, Deborah number, Eckert number, Schmidt, chemical reaction, activation energy, Biot number, Brownian motion, thermophoresis term, velocity ratio term, mass Biot number, concentration relative term, Reynolds number, Darcy number, entropy number.

Furthermore, the skin friction coefficient C_{fx}, the Nusselt number Nu_x and the Sherwood number Sh_x which are quantities of engineering interest are orderly presented as:

$$c_{fx} = \frac{\tau_w}{\rho U_s^2}, N_{ux} = \frac{x q_w}{k(T_w - T_\infty)}, S_{hx} = \frac{x q_m}{D_B (C_w - C_\infty)}, \tag{18}$$

with $\tau_w, q_w,$ and q_w describing the shear stress, surface heat and mass flux in that order. Also,

$$\tau_w = \frac{\mu}{1+\beta}\left[\left(\frac{\partial u}{\partial y}\right) + \alpha\left(u\frac{\partial^2 u}{\partial x \partial y} + v\frac{\partial^2 u}{\partial y^2}\right)\right]_{y=0}, q_w = -\left[\left(k + \frac{16T^3\sigma}{3k^*}\right)\frac{\partial T}{\partial y}\right]_{y=0}, q_m = -D_B\left(\frac{\partial C}{\partial y}\right)_{y=0}, \tag{19}$$

in view of equations (10) and (19), the quantities in (18) respectively becomes (19-21)

$$c_{fx} = \frac{1}{Re_x^{1/2}(1+\beta)}[f''(0) + \zeta[f'(0)f''(0) - f(0)f'''(0)]], \tag{19}$$

$$N_{ux} = -[1 + Rd(1 + (\theta_r - 1)\theta(0))^3]Re_x^{1/2}\theta'(0), \tag{20}$$

$$S_{hx} = -Re_x^{\frac{1}{2}}\phi'(0). \tag{21}$$

2.2 Method Of Solution And Validation

Due to high nonlinearity of the system of the boundary value equations (11-14), a numerical technique via Runge-Kutta-Fehlberg method associated with shooting technique has been adopted for the solution. The details of this technique can be found in Fatunmbi and Okoya (2020), Xu and Lee (2013). The impact of the emerging parameters on the various dimensionless quantities, viz: velocity, temperature, concentration, skin friction coefficient, Nusselt and Sherwood numbers as well as entropy number and Bejan number are analyzed. A comparative analysis of $(-\theta'(0))$ and $-\phi'(0))$ for variations in Nt and Nb with earlier published results of Dalair *et al.*(2015) and Khan & Pop (2010) is analyzed in Table 1 which validate our numerical code. The underlisted are parametric values used unless differently mentioned in specific figures. $Fw = R = 0.5, A = Ec = Q = Q^\star = \zeta = Nb = Nt = \gamma_1 = 0.1, \beta = M = 0.2, E = n = G_1 = G_2 = 0.5, Pr = 7.0, Sc = 1.0, \theta r = 1.3$.

Table 1: Computed values of $-\theta'(0)$ when $Pr = Sc = 10, G_1 = G_2 \to \infty$.

	Dalir *et al.*(2015)	Khan & Pop (2010)	Present	Dalir *et al.*(2015)	Khan & Pop (2010)	Present
Nt		$Nb = 0.1$			$Nb = 0.3$	
0.1	0.95238	0.9524	0.95238	0.25213	0.2522	0.25216
0.3	0.52008	0.5201	0.52008	0.13549	0.1255	0.13551
0.5	0.32105	0.3210	0.32106	0.08328	0.0833	0.08330

3. RESULTS ANALYSIS AND DISCUSSION

The significant contributions of the emerging parameters on the dimensionless quantities are graphically depicted and deliberated in this section. Figure 2a is a sketch showing the combined impacts of the temperature excess ratio θ_r and the Brownian diffusion parameter Nb on the temperature field. As expected, the temperature profile advances with rising values of θ_r. At the same time, the influence of Nb is to thicken the thermal boundary layer and thus leading to a rise in the surface temperature particularly near the stretching sheet. In the existence of Eckert number Ec, the thermal field is strengthened as graphically described in Fig. 2b. In a related sense, the space dependent heat source Q promotes thermal

acceleration due to an additional heat supplied into the flow region. Fig. 2c. is a plot of the thermal field against η for different values of temperature-dependent heat source $Q^{\star}$ in the presence of the surface convection term G_1. It is noticeable that the temperature profile uplifts with a rise in $Q^{\star}$. Such an observation is also noticed for a rise in G_1 due to the fact that convective heating advances with higher thermal Biot number G_1.

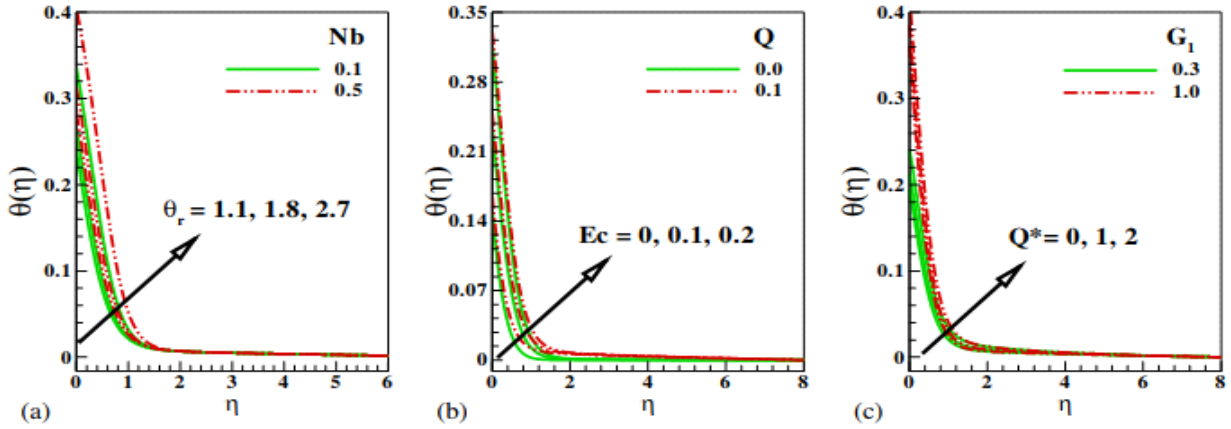

Fig. 2 Temperature profiles for variation in (a) θ_r and Nb (b) Ec and Q (c) $Q^{\star}$ and G_1.

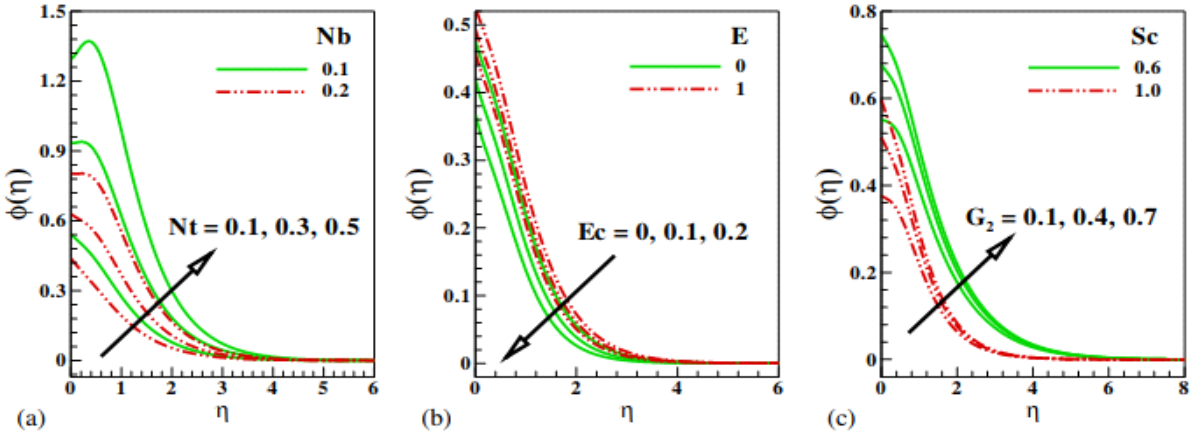

Fig. 3 Concentration field for variations in (a) Nt and Nb (b) E and Ec (c) G_2 and Sc.

Figure 3a depicts that the nanoparticle concentration is raised as the thermophoresis term Nt grows in magnitude whereas an opposite trend is observed with an increase in Nt. A rise in Nb dampen the nanoparticle concentration boundary layer thickness and propels the downfall of the nanoparticle volume fraction. In Fig. 3b, an increase in the activation energy E facilitates the growth of the Jeffrey fluid nanoparticle concentration profile. From Fig. 3c, it clearly shown that the nanoparticles concentration structure uplifts with the higher values of mass Biot number G_2 such behaviour emanated from the fact as G_2 is proportional to h_2 which defines the nano particle concentration coefficient, thus, a growth in h_2 enables an advancement in the nanoparticle concentration profile. On the other hand, The influence of Schmidt number Sc is to diminish the nanoparticle volume fraction.

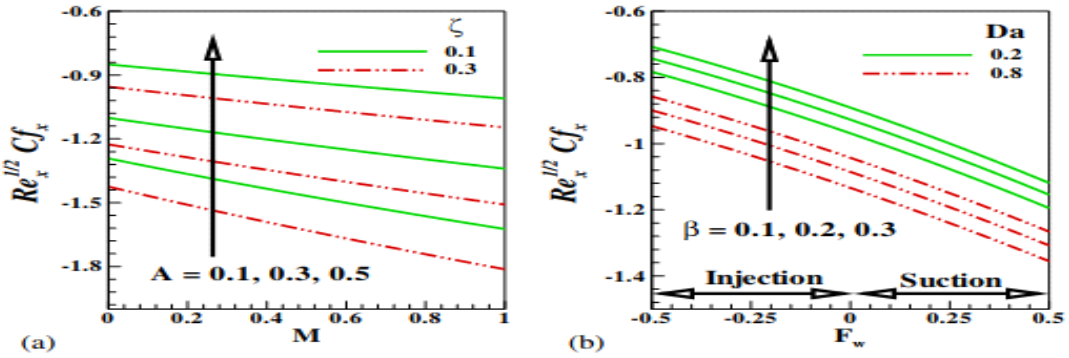

Fig. 4 (a) Skin friction C_{fx} versus M for variation in A and ζ (b) C_{fx} versus F_w for variations in β and Da.

Fig. 4a informs that C_{fx} improves with a rise in the stretching parameter A for any value of M. This trend occurs due to the fact that the free stream velocity moves faster than the stretching velocity with a rise in A such that additional friction is created due to drag between the fluid and the sheet. Contrarily, a rise in the Deborah number ζ reduces C_{fx} irrespective of any value of M while C_{fx} is raises for lower values of M. It is to be pointed out that a growth in ζ is an indication that the Jeffrey nano fluid viscosity is reduced while the fluid elasticity is enabled, in such a situation, the drag force is minimized on the sheet. The pattern in C_{fx} is enhanced when there is a rise in β for both permeable and impermeable sheet and any value of F_w as shown in Fig. 4b. The rise in C_{fx} in respect to β is indicates that the fluid particles require more time to recover from a disturbed state to a stable state.

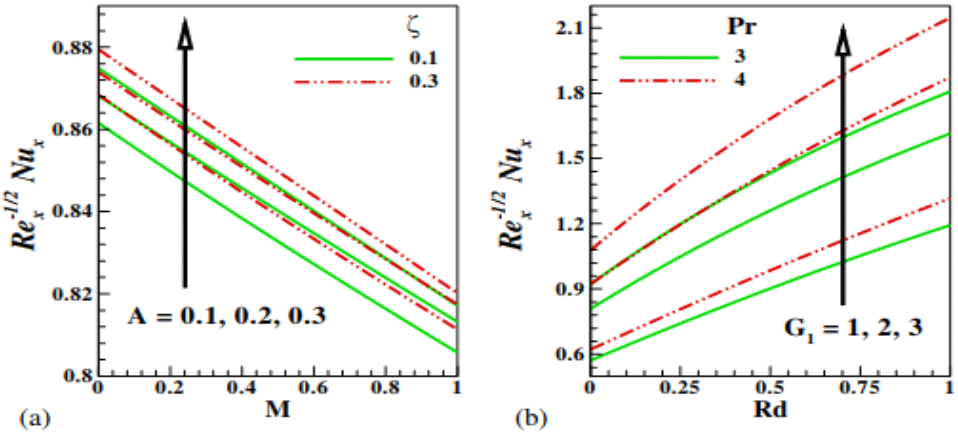

Fig. 5 (a) Nusselt number Nu_x versus M for changes in A and ζ (b) Nu_x versus Rd for changes in G_1 and Pr.

Figure 6a is constructed to show the impact of A,ζ and M on the heat transfer. It is clear from this figure that a growth in the stretching parameter A as well as Deborah number ζ favours the heat transfer rates whereas higher values of the magnetic field term M slow down rate of heat transfer. From Fig. 6b, it conspicuously seen that rising values Pr, thermal Biot number G_1 as well as radiation term Rd energizes heat transfer at the surface. The entropy generation number N_G is increasing due to a rise in the Darcy Da and magnetic field term M as revealed in Fig. 6a. Both Da and M have been found to lower the fluid flow thereby create more friction in the boundary layer which can be attributed to a growth in N_G. Conversely, with higher values of A, there is significant reduction in N_G. Likewise, Fig. 6b shows that N_G is a rising function of nanoparticles diffusion parameter γ_2 and volume fraction concentration relative term ϕ_w. More so, it is evident from Fig. 6c that N_G is enhanced for higher values of β whereas it declines with a rise in ζ

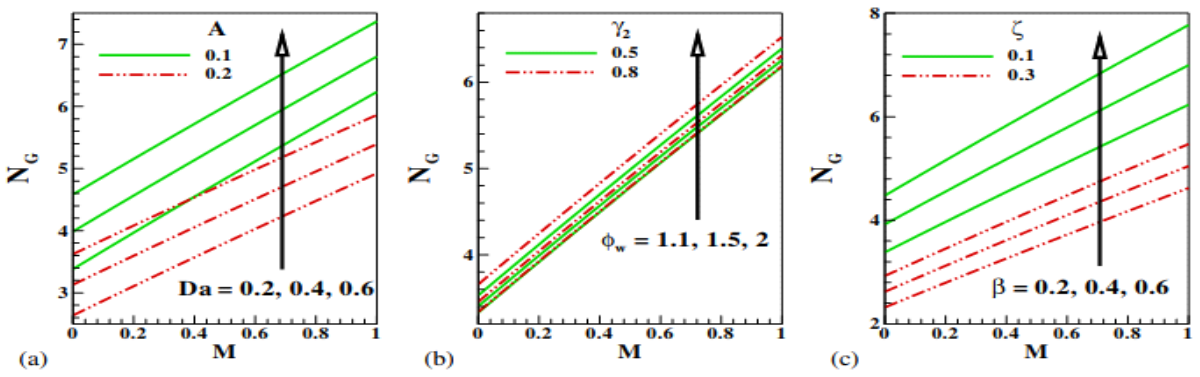

Fig. 6 Entropy number versus M for variations in (a) A & Da (b) ϕ_w & γ_2 (c) β & ζ.

Figure 6 (a-c) describe the plots of Bejan number Be against the magnetic field parameter M for different values of Da, $A, \phi_w, \gamma_2, \beta$ and ζ. Clearly, from Fig. 6a, growing values of Da lowers Be for any value of M, this implies that irreversibility due to fluid friction and magnetic field/Ohmic heating is stronger than that of heat and mass transfer irreversibilities. However, higher values of A shows an opposite behaviour to this fact as noted in this figure. Furthermore, it is pointed out from Fig. 6b that entropy production resulting from heat and mass transfer takes preeminence due to an advancement in Be as ϕ_w and γ_2 increase for any value of M. A similar response is occurs with a rise in the Deborah number ζ as depicted in Fig. 6c.

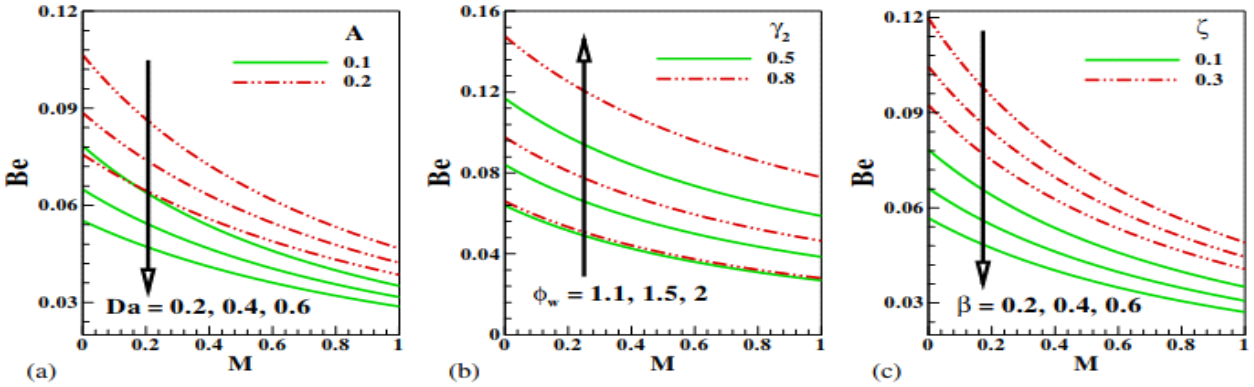

Fig. 7 Bejan number versus M for variation in (a) A & Da (b) ϕ_w & γ_2 (c) β & ζ.

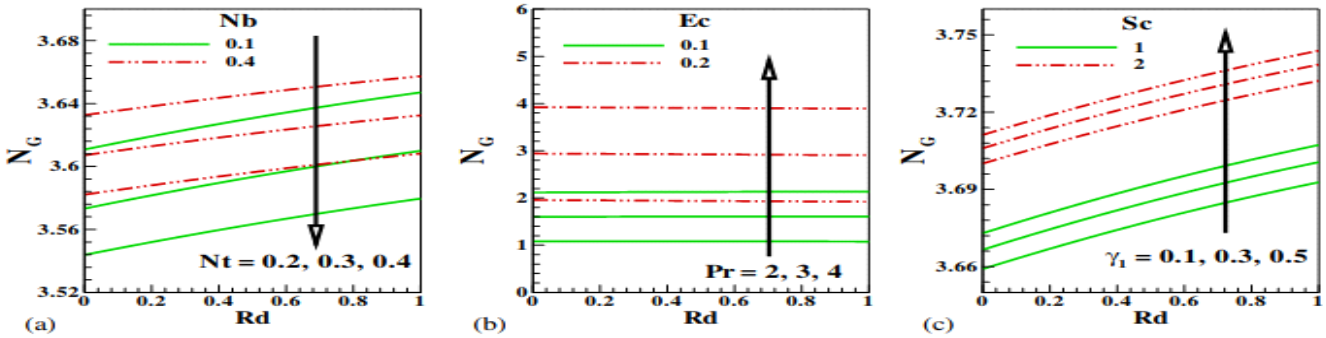

Fig. 8 Entropy number versus radiation term Rd for variations in (a) Nt & Nb (b) Pr & Ec (c) γ_1 & Sc.

Figure 8 (a-c) depict the impact of Nt, Nb, Pr, Ec, γ_1 and Sc on entropy generation number N_G. A rise in Nt significantly reduces N_G as shown in Fig. 10a whereas N_G is energized with higher values of Nb. From Fig. 8b, it is noticeable that both Pr and Ec prompted an advancement in N_G irrespective of the value of radiation parameter Rd. Fig 8c reveals that the entropy number N_G is significantly enhanced with higher values of Sc as well as γ_1..

5. CONCLUSION

The transport of an electrically conducting Jeffrey nanofluid over a permeable stretching sheet in a saturated porous medium with entropy generation analysis has been numerically analyzed in this study. The flow is induced by the stretching sheet in the neighborhoud of a stagnation-point under the influence of nonlinear thermal radiation, chemical reaction associated with activation energy and convective heat and mass flux boundary conditions. The outlining equations have been numerically solved using Runge-Kutta-Fehlberg alongside shooting technique. The results have been validated with published works in the limiting scenarios and found to be strongly related. From the analysis, the following crucial points have been deduced:

• The skin friction coefficient C_{fx} is strengthened for higher values of the ratio of relaxation to retardation times β for both suction/injection term. Likewise, C_{fx} uplifts for growth in the stretching parameter A whereas the trend is reversed for higher values of the Deborah number ζ and Darcy number Da irrespective of the value of M.

• The entropy number N_G is energized for rising values of Da, M, Pr, Ec, Sc, nanoparticles diffusion parameter γ_2 and volume fraction concentration relative term ϕ_w whereas N_G significantly depreciates for higher values ζ.

• The irreversibility due to fluid friction and magnetic field/Ohmic heating is stronger than that of heat and mass transfer irreversibility due to a decline in the Bejan number Be when Da advances, β, Nt, Ec, Pr whereas the trend is changed for rising values of A, ϕ_w, Nb, γ_1, Sc and Deborah number ζ.

• The Jeffrey nanofluid velocity field is a decreasing function of β, M and Da whereas ζ and A strengthens the velocity field. Similarly, the temperature profile is raised for higher values of θr, G_1 Rd and Q while it falls for Pr and Fw.

REFERENCES

Akinbobola, T. E. and Okoya, S. S. (2015). The flow of second grade fluid over a stretching sheet with variable thermal conductivity and viscosity in the presence of heat source/sink. *Journal of Nigeria Mathematical Society, 34*, 331-342

Anderson, H. I. (2002). Slip flow past a stretching surface. *Acta Mechanica 158,* 121- 125.

Batool, K. and Ashraf, M. (2013) Stagnation Point flow and heat transfer of a magneto-micropolar fluid towards a shrinking sheet with mass transfer and chemical reaction. Journal of Mechanics, 29, 411-422.

Bejan, A. (1982). Second law analysis in heat transfer and thermal design, *Adv. Heat Transf., 15*,1-58.

Bejan, A. (1996). *Entropy generation minimization*, (second ed.) CRC, New York.

Choi, S. U. S. and Eastman J. A. (1995). Enhancing thermal conductivity of fluids with nanoparticles, in: Enhancing Thermal Conductivity of Fluids with Nanoparticles, 99-105.

Crane, L. J. (1970). Flow past a stretching plate. *Communicatios Breves, 21*, 645-647.

Dalir, N., Dehsara, M. and Nourazar, S. S. (2015). Entropy analysis for magnetohydrodynamic flow and heat transfer of a Jeffrey nanofluid over a stretching sheet, Energy, 79; 2015; 351-362.

Fatunmbi, E. O. and Adeniyan, A. (2018). Heat and mass transfer in MHD micropolar fluid flow over a stretching sheet with velocity and thermal slip conditions. Open Journal of Fluid Dynamics, 8, 195-215.

Fatunmbi, E. O. and Adeniyan, A. (2020). Nonlinear thermal radiation and entropy generation on steady flow of magneto-micropolar fluid passing a stretchable sheet with variable properties, Results in Engineering, 6, 1-10.

Fatunmbi, E. O. and Adeshina, A. T. (2020). Nonlinear radiative Eyring-Powell nanofluid flow along a vertical Riga plate with exponential varying viscosity and chemical reaction. International Communications in Heat and Mass Transfer, 119, 1-10.

Fatunmbi, E. O. and Okoya, S. S. (2020) Heat transfer in boundary layer magneto-micropolar fluids with temperature-dependent material properties over a stretching sheet, *Advances* in Materials Science and Engineering, 1-11.

Ishak, A., Jafar, K. Nazar, R., and Pop I. (2009). MHD Stagnation point flow towards a stretching sheet, Physica A, 388, 3337-3383.

Khan, W. A, Pop, I. (2010). Boundary-layer flow of a nanofluid past a stretching sheet. Int J Heat Mass Tran; 53:2477e83.

Madhu, M and Kishan, N. (2015). Magnetohydrodynamic mixed convection stagnation-point flow of a power-law non-Newtonian nanofluid towards a stretching surface with radiation and heat source/sink, Journal of Fluids, 2015, Article ID 634186, 14 pages.

Nadeem, S., Zaheer, S. and Fang, T. (2011). Effects of thermal radiation on the boundary layer flow of a Jeffrey fluid over an exponentially stretching surface, Numer Algor, 57,187–205.

Pal, D., Mondal, S., and Mondal, H. (2019). Entropy generation on MHD Jeffrey nanofluid over a stretching sheet with nonlinear thermal radiation using spectral quasilinearisation method, Int. J Ambient Energy, 1-16 .

Ramesh, K . (2018). Effects of viscous dissipation and Joule heating on the Couette and Poiseuille flows of a Jeffrey fluid with slip boundary state of affairs. Propulsion and Power Research, 7(4), 329–341.

Shah, Z., Kumam, P., and Deebani, W. (2020). Radiative MHD Casson Nanofluid flow with Activation energy and chemical reaction over past nonlinearly stretching surface through Entropy generation, Salawu, S. O and Fatunmbi, E. O. (2017). Inherent Irreversibility of Hydromagnetic Third-Grade Reactive Poiseuille Flow of a Variable Viscosity in Porous Media with Convective Cooling, Journal of the Serbian Society for Computational Mechanics, 11(1), 46-58.

Shateyi, S. and Marewo, G. T. (2018). Numerical solution of mixed convection flow of an MHD Jeffery fluid over an exponentially stretching sheet in the presence of thermal radiation and chemical reaction, Open Phys., 16, 249–259.

Xu, L. and Lee, E.W.M. (2013). Variational iteration method for the magnetohydrodynamic flow over a nonlinear stretching sheet. Abst Appl Anal, 1-5.